Article

Highly-efficient longitudinal second-harmonic generation from doubly-resonant AlGaAs nanoantennas

Lei Xu [1], Mohsen Rahmani [2], Daria Smirnova [2,3],Khosro Zangeneh Kamali[2], Guoquan Zhang[4], Dragomir Neshev[2], and Andrey E. Miroshnichenko[1]

[1]   School of Engineering and Information Technology, University of New South Wales, Canberra ACT 2600, Australia

[2]   Nonlinear Physics Centre, Research School of Physics and Engineering, The Australian National University, Canberra, ACT 0200 Australia

[3]   Institute of Applied Physics, Russian Academy of Sciences, Nizhny Novgorod 603950, Russia

[4]   The MOE Key Laboratory of Weak-Light Nonlinear Photonics, School of Physics and TEDA Applied Physics Institute, Nankai University, Tianjin 300457, China

*   Correspondence: andrey.miroshnichenko@unsw.edu.au

Abstract: We design an asymmetric nonlinear optical nanoantenna composed of a dielectric nanodisk and an adjacent nanobar. The proposed composite structure made of AlGaAs exhibits resonant response at both the fundamental and doubled frequencies. Being driven by the strong magnetic dipole resonance at the pump wavelength and a high-quality mode at the harmonic wavelength, the efficient second-harmonic radiation is generated predominantly along the vertical directions under the normally incident plane-wave excitation.

Keywords: Scattering; Second-harmonic generation; Mie resonance; Nanoantenna; Multipolar interference.

---

1. Introduction

Nonlinear nanophotonics is a rapidly developing research field with various applications including nonlinear light sources [1], ultrafast chip-based optoelectronic devices [2], spectroscopy [3], bioimaging and sensing [4]. Exploiting nonlinear optical effects in nanostructures plays an important role in the implementation of miniature nonlinear photonic components for further integration of multiple optical functionalities into a single compact optical chip. On this purpose, nonlinear nanoplasmonics has been widely studied both theoretically and experimentally during the last decade [5–10]. However, its performance is restricted by the high Ohmic losses, small mode volumes and low laser damage threshold. All-dielectric nanostructures offer unique opportunities to boost the nonlinear effects due to the strong near-field enhancement associated with the excitation of Mie-type resonances [11,12]. Via engineering and control over the optically-induced electric and magnetic resonances in all-dielectric nanostructrues, both high nonlinear conversion efficiency and directivity of the harmonic radiation pattern can be achieved. Nanostructures made of high-index semiconductors with a strong nonlinear response, such as Si, Ge which possess a large third-order susceptibility, have been investigated widely for third-harmonic generation, showing huge nonlinear enhancement when exciting the nanostructure in the vicinity of Mie resonances, particularly, magnetic dipole (MD) resonance [13], Fano resonance or collective modes [14–16], and anapole states [17–20]. In contrast to the third-order nonlinearity, Si and Ge do not possess bulk second-order nonlinearity due to their centrosymmetric crystalline structure [21]. However, III-V semiconductors, such as GaAs or AlGaAs show a strong second-order nonlinear response due to their large bulk $\chi^{(2)}$ coefficient. By engineering the AlGaAs alloy composition, two-photon absorption can be avoided at the telecommunication wavelengths, enabling high transparency in a

broad spectral window from visible to far infrared. Both theoretical and experimental studies have been performed to enhance the second-harmonic generation (SHG) process in GaAs or AlGaAs Mie resonators [22–27]. The SHG from AlGaAs nanoantennas has been predicted to reach conversion efficiency of 10^{-3}, and later efficiency of 10^{-4} was measured experimentally by exploiting the magnetic dipole (MD) resonance [22,25]. However, when employing AlGaAs structures, despite of high conversion efficiency, there were no emitted second-harmonic (SH) signal observed in both the forward and backward normal directions. The absence of the emission at normal directions is due to the specific nonlinear susceptibility tensor of [100]-grown zinc-blend AlGaAs crystalline structures, which only contains off-diagonal elements $\chi^{(2)}_{ijk}$ with $i \neq j \neq k$. It limits the collected nonlinear signal and restricts many photonic applications, e.g. highly-efficient nonlinear light sources and nonlinear spectroscopy.

In this work, we present a theoretical study on the resonant multipolar effects in AlGaAs nanoantennas in both linear and nonlinear responses. Then we propose and design an asymmetric AlGaAs nanoantenna composed of a nanodisk and an adjacent nanobar. Under normally incident pump, our nanoantenna supports resonant responses at both the fundamental and harmonic wavelengths, enabling a high second-harmonic conversion efficiency of the order of 10^{-3} at the pump intensity of $I_0 = 1$ GW/cm^2, and also normal SH emission due to the the specifically distributed induced nonlinear currents and resonant modes supported by both nanodisk and nanobar. Such highly-efficient longitudinal SH emission has not been realized in [100]-grown AlGaAs nanoantennas to date. Our results may offer new opportunities for the design of new types of novel nonlinear photonic metadevices.

2. Results and Discussion

2.1. Theoretical model and numerical simulations

In our theoretical model, we fixed the thickness of our nanostructures to be h_0=400 nm. The pump is y-polarized with a wavelength of 1550 nm. The widely-used [100]-grown AlGaAs material is considered as the platform for our nanostructures. The second-order nonlinear susceptibility tensor of [100]-grown AlGaAs, possessing a zinc blend crystalline structure, is anisotropic and has only off-diagonal elements $\chi^{(2)}_{ijk}$ with $i \neq j \neq k$. Thus, in the principal-axis system of the crystal, the *i*th component of the nonlinear polarization at the SH frequency is given by

$$P_i^{2\omega} = \epsilon_0 \chi^{(2)}_{ijk} E_j^\omega E_k^\omega. \tag{1}$$

We use FEM solver in COMSOL Multiphysics in the frequency domain to model both the linear and nonlinear responses of such nanoantennas. First, we simulate the linear scattering at the fundamental frequency. The bulk nonlinear polarization induced inside the particle is then employed as a source for the electromagnetic simulation to obtain the generated SH field. The value of $\chi^{(2)}_{ijk}$ in the simulation is 100 pm/V [22]. The material dispersion of AlGaAs is deduced from Refs. [28,29].

2.2. Linear and nonlinear responses from a single AlGaAs nanodisk

The electric and magnetic Mie resonances in all-dielectric nanostructures allow for flexibly engineering the multipolar excitation and control of the optical responses for enhancing the near-field interactions and far-field radiation shaping. Through a geometric tuning, the nanoantenna can support resonant effects at several wavelengths simultaneously. We first optimize our nanoantennas to support strong resonant responses at both 1550 nm and 775 nm, corresponding to the pump and harmonic wavelengths in our case. Figure 1 shows the geometrically-scanned linear scattering characteristics of a free-standing AlGaAs nanodisk under normal plane wave excitation. As can be seen in Figure 1, a broad mode (Mode A) dominated by MD resonance associated with partly excited electric dipole (ED) resonance is obtained for nanodisk of radius $r_0 = 215$ nm at the fundamental

wavelength. This mode allows for a strong near-field enhancement with confined electromagnetic energy inside the nanodisk, as shown in Figure 2(a-c). At the SH wavelength, the scattering spectrum shows a sharp peak corresponding to a resonant mode (Mode B) near $r_0 = 215$ nm. This mode is formed by the excitation of and interference between ED, MD, electric quadrupole (EQ), and electric octupole (EO) resonances. By calculating the complex frequency of the eigenmodes using FEM solver through Eigenfrequency analysis in COMSOL Multiphysics, the Q factor of mode B is estimated to be 52. These high-quality modes supported by the nanoantenna results in an enhanced near-field distributions, as shown in Figure 2(e-g). Further investigation of the far-field pattern shows that both radiation patterns at these two wavelengths are characterized by a main lobe in the forward directions, featuring the Kerker's condition due to the interference between the excited ED and MD resonances. While the slightly narrower lobe for the pattern at SH wavelength is due to the suppression of the side-lobe scattering based on the interference between the same type of excited multipoles of different orders (ED, EQ, EO).
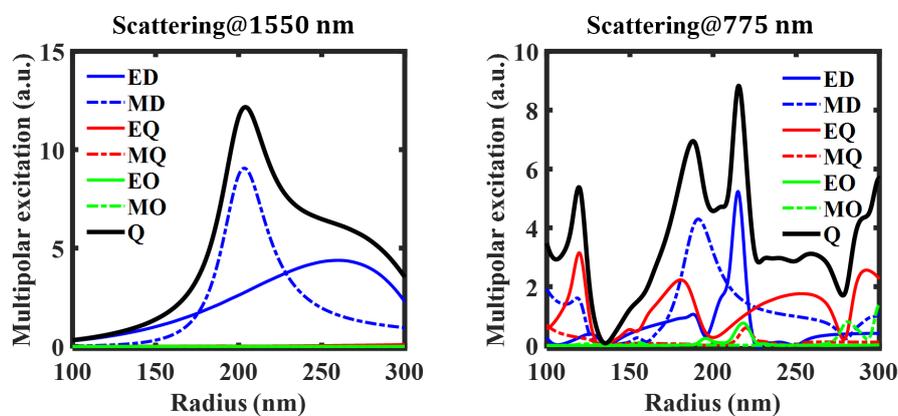

Figure 1. Multipolar decomposition of linear light scattering by AlGaAs nanodisks with different radii for normal plane wave incidence at the wavelength of (a) =1550 nm and (b)λ =775 nm, respectively.

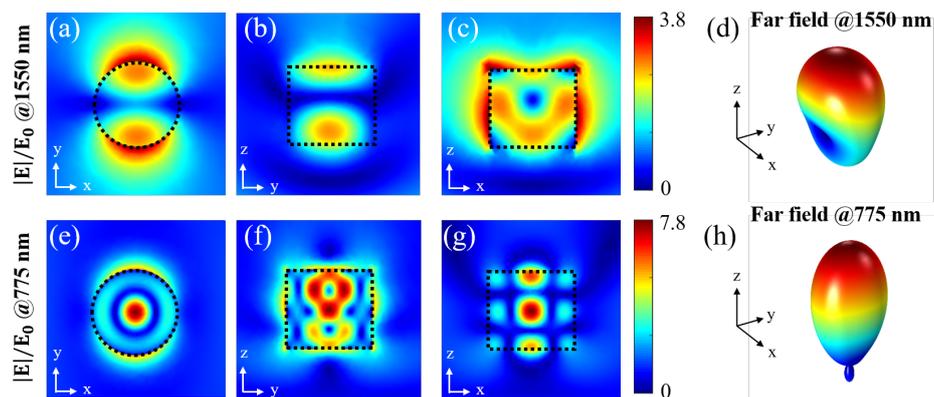**Figure 2.** Near-field distributions of the electric field magnitude for nanodisk radius being r_0 =215 nm at the pump wavelength of (a) =1550 nm and (b)λ =775 nm, respectively.

Optically pumping the nanoantenna in the vicinity of Mode A, and simultaneously exciting the resonant multipolar response driven by Mode B during the nonlinear process allow achieving spectral and spatial mode overlap at both fundamental and SH wavelengths. In this case the SH conversion efficiency is expected to be boosted, as well as achieving longitudinal SH emission based on the multipolar interference effect. It is worth mentioning that the nanodisk supports other modes around the SH wavelength 775 nm besides mode B. These modes are not excited under normal plane wave incidence, while they can be excited under proper pump irradiation conditions. In the following, we

will focus on exploring the SHG process in the vicinity of the above-mentioned Mode A (near the pump wavelength) and Mode B (near the harmonic wavelength) to achieve doubly-resonant normal SH emission in AlGaAs nanoantennas.

The generated nonlinear multipoles inside the nanoantenna are driven by the induced nonlinear currents. Thus, by controlling the induced nonlinear currents, we can further obtain excitation of specific mode, i.e., combination of and interferences between several specific nonlinearly generated multipoles, to enable desirable directivity of the radiation pattern as well as resonantly-enhanced conversion efficiency.

To enable strong resonant response at 775 nm driven by Mode A during the nonlinear process, one possible method is to generate nonlinear polarization within the transverse plane, imitating the mode polarization distribution, which is similar to the case when using normal plane wave irradiation. The second-order nonlinear susceptibility tensor of the [100] grown AlGaAs possesses a zinc-blend crystalline structure containing only off-diagonal elements $\chi^{(2)}_{ijk}$ with $i \neq j \neq k$. Thus, in order to induce the nonlinear polarization within the transverse plane, the excited MD resonance needs to be rotated to along $\pi/4$ to the transverse plane. For our designed AlGaAs nanodisk with similar size in each direction, this can be simply achieved by tilting the incident pump. For example, optically pumping along $\pi/4$ will excite a MD oriented along $pi/4$, resulting in induced nonlinear polarization vectors mainly within the transverse plane. Based on Figure 1(b), this induced nonlinear polarization is expected to possess strong resonant response at 775 nm driven by Mode A. The calculated near-field distributions at fundamental and harmonic wavelengths are shown in Figure 3(a) and Figure 3(b), respectively. It is clearly shown that the SH near-field distribution resembles Mode B in Figure 2 revealing the resonant response of SH emission driven by Mode B. Figure 3(c) shows the SH far-field pattern. The SH conversion efficiency is estimated to be of the order of 10^{-3} using a pump intensity of $I_0 = 1$ GW/cm^2, demonstrating both high efficiency and normal emission in this case. This feature has been previously mentioned in Ref. [26].

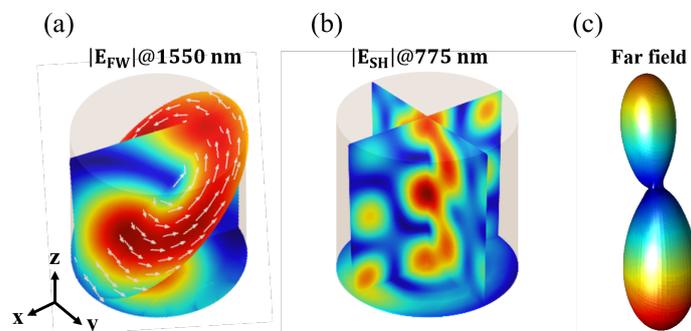| (a)	(b)	(c)
$|E_{FW}|$@1550 nm	$|E_{SH}|$@775 nm	Far field

Figure 3. Near-field distributions of electric field magnitude at fundamental wavelength (a) and harmonic wavelength (b), respectively. (c) gives the SH radiation pattern.

This can also be interpreted from the overlap between the nonlinear currents and the specified mode, which is defined as

$$\zeta = \frac{\int |\mathbf{E}_r^* \cdot \mathbf{J}_i|^2 dV}{\int |\mathbf{E}_r|^2 dV| \int |\mathbf{J}_i|^2 dV} \,. \tag{2}$$

where $\mathbf{E}_r$ is the resonant mode at the harmonic wavelength, and $\mathbf{J}_i$ is the induced nonlinear current by a given pump.

As shown in Figure 4, the maximum SH conversion efficiency happens when the overlap reaches its maximum. The multipolar excitation varies with increasing pump tilt angle θ, resulting in reshaping of the SH far-field pattern (see Figure 2(c) and Figure 4(c,d)). A strong normal SH emission takes place under pump beam tilt angle $\theta = \pi/4$, where the overlap between the nonlinear currents and Mode B is around 0.3 (Figure 2(c)). Compared with the multipolar excitation shown in Figure 1(b) and far-field pattern shown in Figure 2(h), the lack of excitation of sizable MD and
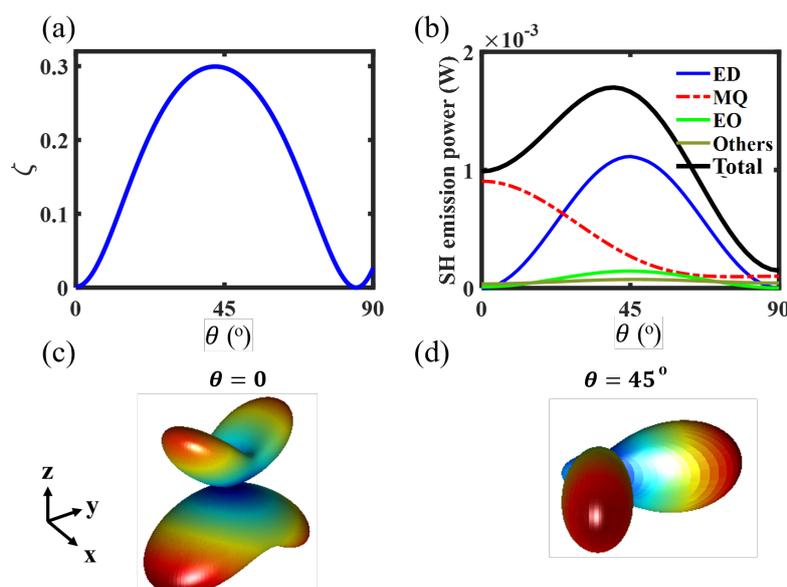
Figure 4. (a) Calculated overlap ζ for different pump tilt angle. (b) The multipolar structure of SH emission with different pump tilt angle.

EQ further weakens the Kerker's condition and leads to a SH emission pattern in both forward and backward directions (as shown in Figure 3(c)).

The unique tensorial susceptibility of AlGaAs material enables the polarization-dependent of the nonlinear emission on the pump [25,27]. By simply varying the angle θ_c between the crystalline axis and laboratory coordinate x (or y) axis within the transverse plane, the nonlinearly generated electric and magnetic multipoles can be tuned slightly. The SH conversion efficiency increases with increasing θ_c from 0° to 45°. This polarization-dependence of SHG also provides a simple method to determine the crystalline orientation of AlGaAs nanoantennas [30]. Importantly, the SH emission maintains high directivity, i.e., normal emission under different rotating angle θ_c, as shown in Figure 5.
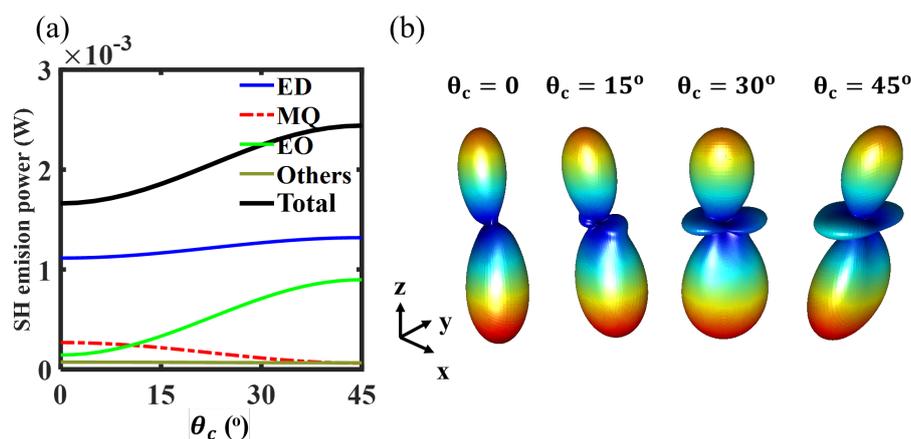

Figure 5. Nonlinear emission under oblique pump incidence with $\theta = 45°$. (a) Nonlinear multipolar excitation for different rotating angle θ_c. (b) The far-field patterns for different rotating angle θ_c.

However, considering practicability where objectives are used to both excite the nanoantenna and collect the signals [25], after tilting the incident pump experimentally, the collection of the normal harmonic emission remains a problem. Approaches to obtain normal harmonic emission by normal pump incidence are yet to be developed.

2.3. Longitudinal SHG through a doubly-resonant asymmetric AlGaAs nanoantenna

As discussed above, by exciting 45°-oriented MD resonance at the fundamental wavelength, it is possible to induce a parallel-oriented nonlinear polarization from AlGaAs nanoantenna, and furthermore obtain the resonant response of SH emission driven by Mode B at the harmonic wavelength. Unfortunately, for a nanodisk under normal pump incidence, the excitation of 45°-oriented MD resonance is not possible due to the symmetry protection. However, by breaking the symmetry of our nanoantenna, it is possible to control the orientation of excited MD resonance. Here, we further introduce an adjacent nanobar near the nanodisk to control the MD excitation. The schematic of the designed nanoantenna is shown in Figure 6(a). It is worth noting that the material and size of the nanobar are also flexible and not restricted to AlGaAs in this approach. Here, for practical purposes, the thickness and material is set to be the same as the nanodisk, and the size of the nanobar is chosen to be length L=200 nm, width w=900 nm. Under normal pump incidence, the MD supported by the nanodisk can be engineered through the interaction with the ED resonance supported by the nanobar. As a result, the MD resonances is re-oriented along 45° to the in-plane direction, similar to the case where oblique pump excitation on a single nanodisk (see Figure 3(a)). Thus, in the vicinity of Mode B supported by the nanodisk, this MD resonance will further excite strong multipolar resonances during the nonlinear process, leading to highly-efficient normal nonlinear emission.
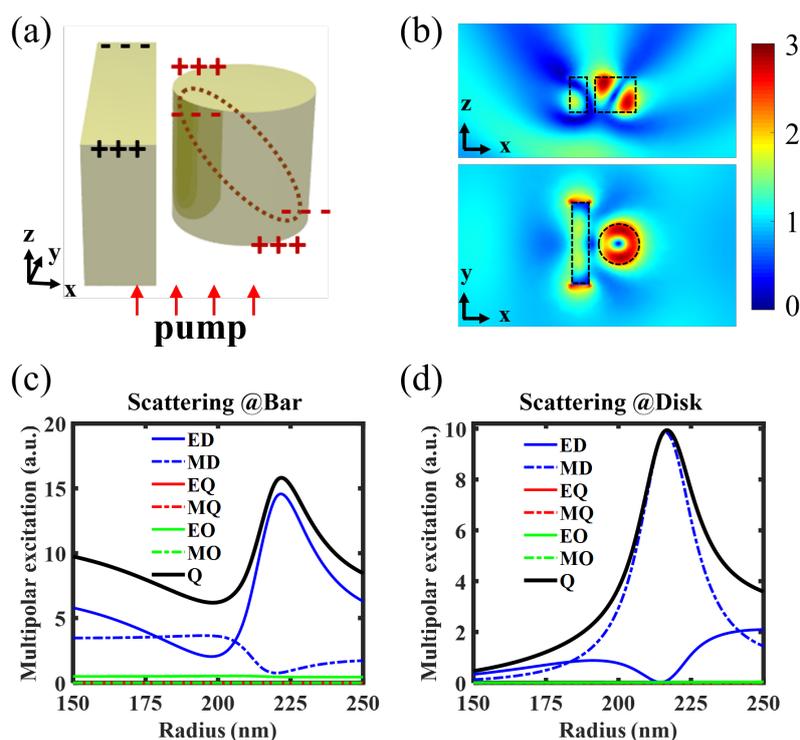

Figure 6. (a) Schematic of designed asymmetric AlGaAs nanoantennas. (b) Near-field distribution of electric field under normal plane wave pump with =1550 nm. (c) Multipolar excitations within the nanobar as a function of the disk radius. (d) Multipolar excitation within the nanodisk as a function of the disk radius.

Figure 6(b) shows the near-field distributions at the fundamental wavelength, the 45°-oriented circular field distribution reveals the excitation of MD resonance along 45° to the in-plane direction. We further use the internal field inside the nanoantenna to perform the multipolar decomposition for the nanodisk and nanobar separately, as shown in Figure 6(c,d). For the disk radius r_0 =215 nm, an ED resonance is excited within the nanobar, while a MD resonance is excited within the nanodisk with the suppression of ED resonance, exhibiting also anapole state excitation for the disk radius

$r_0 =$215 nm. This will further benefit to our target to achieve highly-efficient normal emission driven by Mode B supported by the nanodisk: for nonlinear process, MD resonance has been well-known for its ability to boost the nonlinear process due to the near-field enhancement inside the nanostructure, while for ED resonance, most of the electric energy is located near the edges of nanostructure, its ability to enhance the nonlinear process is restricted.

We first investigate the SH emission enhancement through such doubly-resonant nanoantennas. Figure 7(a) gives the calculated SH emission power as a function of the disk radius. By optically pumping near MD resonance, we are able to obtain strong SH enhancement at the harmonic wavelength in the vicinity of Mode A position $r_0 =$215 nm. Meanwhile, an emission peak also occurs around disk radius of 202.5 nm. This peak is driven by other mode supported by the nanoantenna at this position, resulting from the alignment of the induced nonlinear current and the mode. However, the far-field pattern from this strong SH emission possess nearly null in the forward and backward directions, as shown in the inset of Figure 7(a), different from the SH emission pattern driven by Mode B (shown in the following Figure 8).
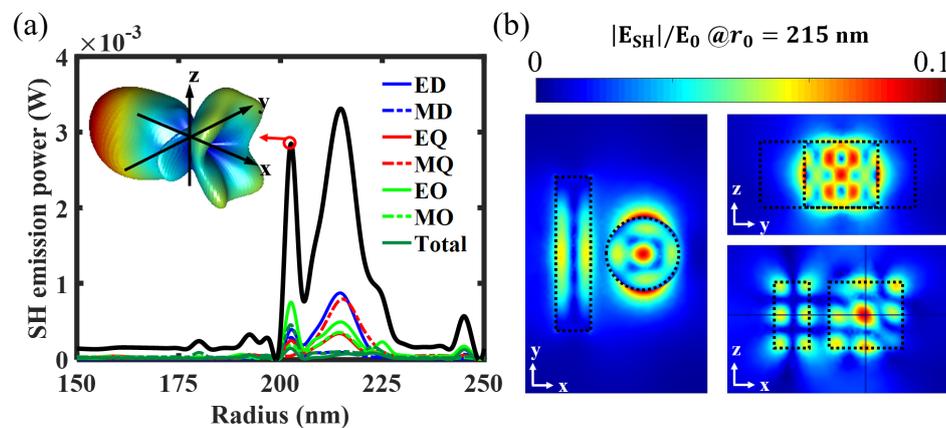

Figure 7. (a) Calculated SH emission power and the nonlinear multipolar structure with different disk radii. Inset shows the corresponding SH far-field pattern for disk radius r_0=202.5 nm. (b) Near-field distributions of the SH electric field magnitude for disk radius r_0=215 nm. $\theta_c = 0$.

Figure 7(b) shows the near-field distributions corresponding to the SH emission peak at disk radius r_0=215 nm. It resembles the field of Mode B in Figure 2(e-g), revealing the resonant response driven by Mode B at the harmonic wavelength. By further tuning the crystalline angle θ_c, we are able to slightly tune the nonlinearly generated multipoles. Figure 8(a) shows the nonlinear multipolar excitation as a function of the rotating angle θ_c. Generally, with increasing θ_c from $0°$ to $45°$, the excitation of electric dipole resonance increases with other types of multipoles remain almost unchanged during the nonlinear process. These multipolar excitations further enable longitudinal SH emissions for different θ_c, and a stronger side-lobe suppression in the far-field radiation patterns for larger θ_c (Figure 8(b)).

3. Conclusions

In summary, we have demonstrated numerically SHG enhancement based on doubly-resonant AlGaAs nanoantennas. By exploiting the modes supported at the harmonic wavelength, it is possible to shape the SH emission pattern and achieve high directivity. Specifically, we have focused on the SHG process driven by the MD resonance at the fundamental wavelength and a high-quality mode at the harmonic wavelength, which leads to normal emission due to the multipolar interference effect. It is shown that by introducing a nanobar adjacent to the nanodisk, it is possible to achieve highly-efficient longitudinal SH emission under normal pump incidence. Our results demonstrate a method to enhance the nonlinear emission and shape the nonlinear radiation pattern through the
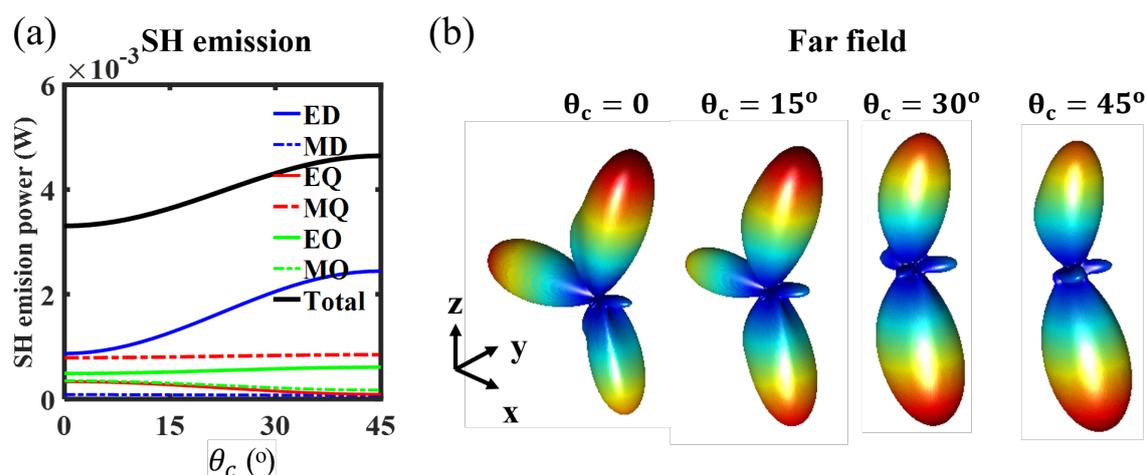
Figure 8. (a) Calculated SH emission power and the nonlinear multipolar structure as a function of θ_c. (c) The near-field profiles at fundamental wavelength. (d) Calculated SHG efficiency and the nonlinear multipolar structure with different disk radii. The inset shows the radiation diagram of the SH field at the peak.

control over the induced nonlinear currents, that can be useful for applications, such as efficient nonlinear light sources, and nonlinear spectroscopy.

References

1. Solntsev, A.; Carletti, L.; Xu, L.; Poddubny, A.; De Angelis, C.; Leo, G.; Kivshar, Y.; Neshev, D.N.; Sukhorukov, A.A. Quantum-classical correspondence for photon-pair generation in nonlinear dielectric nano-resonators. Nonlinear Photonics. Optical Society of America, 2016, pp. NT3A–4.

2. van Sark, W.G.; de Wild, J.; Rath, J.K.; Meijerink, A.; Schropp, R.E. Upconversion in solar cells. *Nanoscale Res. Lett.* **2013**, *8*, 81.

3. Bautista, G.; Kauranen, M. Vector-field nonlinear microscopy of nanostructures. *ACS Photonics* **2016**, *3*, 1351–1370.

4. DaCosta, M.V.; Doughan, S.; Han, Y.; Krull, U.J. Lanthanide upconversion nanoparticles and applications in bioassays and bioimaging: A review. *Analytica chimica acta* **2014**, *832*, 1–33.

5. Klimov, V. *Nanoplasmonics: Fundamentals and applications*; Pan Stanford, 2012.

6. Lippitz, M.; van Dijk, M.A.; Orrit, M. Third-harmonic generation from single gold nanoparticles. *Nano Lett.* **2005**, *5*, 799–802.

7. Aouani, H.; Rahmani, M.; Navarro-Cía, M.; Maier, S.A. Third-harmonic-upconversion enhancement from a single semiconductor nanoparticle coupled to a plasmonic antenna. *Nat. Nanotechnol.* **2014**, *9*, 290–294.

8. Kim, S.; Jin, J.; Kim, Y.J.; Park, I.Y.; Kim, Y.; Kim, S.W. High-harmonic generation by resonant plasmon field enhancement. *Nature* **2008**, *453*, 757–760.

9. Hanke, T.; Cesar, J.; Knittel, V.; Trugler, A.; Hohenester, U.; Leitenstorfer, A.; Bratschitsch, R. Tailoring spatiotemporal light confinement in single plasmonic nanoantennas. *Nano Lett.* **2012**, *12*, 992–996.

10. Hentschel, M.; Utikal, T.; Giessen, H.; Lippitz, M. Quantitative modeling of the third harmonic emission spectrum of plasmonic nanoantennas. *Nano Lett.* **2012**, *12*, 3778–3782.

11. Kuznetsov, A.I.; Miroshnichenko, A.E.; Brongersma, M.L.; Kivshar, Y.S.; Luk'yanchuk, B. Optically resonant dielectric nanostructures. *Science* **2016**, *354*, aag2472.

12. Smirnova, D.; Kivshar, Y.S. Multipolar nonlinear nanophotonics. *Optica* **2016**, *3*, 1241–1255.

13. Shcherbakov, M.R.; Neshev, D.N.; Hopkins, B.; Shorokhov, A.S.; Staude, I.; Melik-Gaykazyan, E.V.; Decker, M.; Ezhov, A.A.; Miroshnichenko, A.E.; Brener, I.; Fedyanin, A.A.; Kivshar, Y.S. Enhanced Third-Harmonic Generation in Silicon Nanoparticles Driven by Magnetic Response. *Nano Lett.* **2014**, *14*, 6488–6492.

14. Yang, Y.; Wang, W.; Boulesbaa, A.; Kravchenko, I.I.; Briggs, D.P.; Puretzky, A.; Geohegan, D.; Valentine, J. Nonlinear Fano-resonant dielectric metasurfaces. *Nano Lett.* **2015**, *15*, 7388–7393.

15. Shorokhov, A.S.; Melik-Gaykazyan, E.V.; Smirnova, D.A.; Hopkins, B.; Chong, K.E.; Choi, D.y.; Shcherbakov, M.R.; Miroshnichenko, A.E.; Neshev, D.N.; Fedyanin, A.A.; Kivshar, Y.S. Multifold Enhancement of Third-Harmonic Generation in Dielectric Nanoparticles Driven by Magnetic Fano Resonances. *Nano Lett.* **2016**, *16*, 4857–4861.

16. Chen, S.; Rahmani, M.; Li, K.F.; Miroshnichenko, A.; Zentgraf, T.; Li, G.; Neshev, D.; Zhang, S. Third Harmonic Generation Enhanced by Multipolar Interference in Complementary Silicon Metasurfaces. *ACS Photonics* **2018**, p. acsphotonics.7b01423.

17. Grinblat, G.; Li, Y.; Nielsen, M.P.; Oulton, R.F.; Maier, S.A. Enhanced third harmonic generation in single germanium nanodisks excited at the anapole mode. *Nano Lett.* **2016**, *16*, 4635–4640.

18. Shibanuma, T.; Grinblat, G.; Albella, P.; Maier, S.A. Efficient Third Harmonic Generation from Metal–Dielectric Hybrid Nanoantennas. *Nano Lett.* **2017**, *17*, 2647–2651.

19. Vabishchevich, P.P.; Liu, S.; Sinclair, M.B.; Keeler, G.A.; Peake, G.M.; Brener, I. Enhanced second-harmonic generation using broken symmetry III–V semiconductor fano metasurfaces. *ACS Photonics* **2018**.

20. Xu, L.; Rahmani, M.; Zangeneh Kamali, K.; Lamprianidis, A.; Ghirardini, L.; Sautter, J.; Camacho-Morales, R.; Chen, H.; Parry, M.; Staude, I.; Zhang, G.; Neshev, D.; Miroshnichenko, A.E. Boosting third-harmonic generation by a mirror-enhanced anapole resonator. *Light: Science & Applications* **2018**, *7*, 44.

21. Boyd, R.W. *Nonlinear optics*; Elsevier, 2003.

22. Carletti, L.; Locatelli, A.; Stepanenko, O.; Leo, G.; De Angelis, C. Enhanced second-harmonic generation from magnetic resonance in AlGaAs nanoantennas. *Opt. Express* **2015**, *23*, 26544.

23. Gili, V.; Carletti, L.; Locatelli, A.; Rocco, D.; Finazzi, M.; Ghirardini, L.; Favero, I.; Gomez, C.; Lemaître, A.; Celebrano, M.; De Angelis, C.; Leo, G. Monolithic AlGaAs second-harmonic nanoantennas. *Opt. express* **2016**, *24*, 15965–15971.

24. Liu, S.; Sinclair, M.B.; Saravi, S.; Keeler, G.A.; Yang, Y.; Reno, J.; Peake, G.M.; Setzpfandt, F.; Staude, I.; Pertsch, T.; Brener, I. Resonantly enhanced second-harmonic generation using III–V semiconductor all-dielectric metasurfaces. *Nano Lett.* **2016**, *16*, 5426–5432.

25. Camacho-Morales, R.; Rahmani, M.; Kruk, S.; Wang, L.; Xu, L.; Smirnova, D.A.; Solntsev, A.S.; Miroshnichenko, A.; Tan, H.H.; Karouta, F.; Naureen, S.; Vora, K.; Carletti, L.; De Angelis, C.; Jagadish, C.; Kivshar, Y. Nonlinear generation of vector beams from AlGaAs nanoantennas. *Nano Lett.* **2016**, *16*, 7191–7197.

26. Carletti, L.; Locatelli, A.; Neshev, D.; De Angelis, C. Shaping the Radiation Pattern of Second-Harmonic Generation from AlGaAs Dielectric Nanoantennas. *ACS Photonics* **2016**, *3*, 1500–1507.

27. Ghirardini, L.; Carletti, L.; Gili, V.; Pellegrini, G.; Duò, L.; Finazzi, M.; Rocco, D.; Locatelli, A.; De Angelis, C.; Favero, I.; others. Polarization properties of second-harmonic generation in AlGaAs optical nanoantennas. *Optics letters* **2017**, *42*, 559–562.

28. Shoji, I.; Kondo, T.; Kitamoto, A.; Shirane, M.; Ito, R. Absolute scale of second-order nonlinear-optical coefficients. *JOSA B* **1997**, *14*, 2268–2294.

29. Ohashi, M.; Kondo, T.; Ito, R.; Fukatsu, S.; Shiraki, Y.; Kumata, K.; Kano, S. Determination of quadratic nonlinear optical coefficient of Al x Ga1- x As system by the method of reflected second harmonics. *Journal of applied physics* **1993**, *74*, 596–601.

30. Camacho-Morales, R.; Bautista, G.; Zang, X.; Xu, L.; Turquet, L.; Miroshnichenko, A.; Lamprianidis, A.; Rahmani, M.; Neshev, D.N.; Kauranen, M. Resonant harmonic generation in AlGaAs nanoantennas using cylindrical vector beams. CLEO: QELS_Fundamental Science. Optical Society of America, 2018, pp. FF1E–6.